IOP Publishing New J. Phys. 26 (2024) 093034 https://doi.org/10.1088/1367-2630/ad7282

New Journal of Physics
The open access journal at the forefront of physics

Deutsche Physikalische Gesellschaft DPG
IOP Institute of Physics

Published in partnership with: Deutsche Physikalische Gesellschaft and the Institute of Physics

OPEN ACCESS

RECEIVED
8 April 2024

REVISED
19 August 2024

ACCEPTED FOR PUBLICATION
22 August 2024

PUBLISHED
24 September 2024

PAPER

Evaluation of single silicon vacancy centers in nanodiamonds created by ion implantation at cryogenic temperatures

Konosuke Shimazaki[1], Kazuki Suzuki[1], Kengo Sakamoto[1], Yudai Okashiro[1], Hiroshi Abe[2], Takeshi Ohshima[2,3], Hideaki Takashima[1,4] and Shigeki Takeuchi[1,*]

[1] Department of Electronic Science and Engineering, Kyoto University, Kyotodaigakukatsura, Nishikyo-ku, Kyoto 615-8510, Japan
[2] National Institutes for Quantum Science and Technology (QST), Quantum Materials and Application Research Center (QUARC), 1233 Watanuki, Takasaki, Gunma 370-1292, Japan
[3] Department of Materials Science, Tohoku University, Aoba, Sendai, Miyagi 980-8579, Japan
[4] Chitose Institute of Science and Technology, 758-65, Chitose, Hokkaido 066-8655, Japan
[*] Author to whom any correspondence should be addressed.

E-mail: takeuchi@kuee.kyoto-u.ac.jp

Keywords: color center in diamond, silicon vacancy center, single photon emitter

Abstract

Silicon vacancy (SiV) centers in diamonds have attracted much attention because of their stability and narrow emission linewidth, and are promising for applications in quantum information technology. SiV-center-encapsulated nanodiamonds have also attracted much attention because of their potential to be coupled to various photonic devices. One efficient way to fabricate nanodiamonds that contain SiV centers is Si ion implantation into nanodiamonds. However, the evaluation of a single SiV center in a nanodiamond produced by this method at low temperatures has not been performed. In this study, we report on the optical properties of a single SiV center in a nanodiamond produced by ion implantation at cryogenic temperatures. The emission spectrum from a single SiV center ($g^2(0) = 0.19$) was observed with four distinct fine splittings of the zero-phonon line (ZPL) at 4 K. At an excitation power of 50 μW, the full width at half maximum of the ZPL reached the spectrometer resolution limit (0.09 nm). The temperature dependence of the emission peak is consistent with that of the emission coming from an SiV center under high strain. The results obtained in this work suggest that nanodiamonds containing single SiV centers formed using this method will be an important building block for the realization of quantum information applications.

1. Introduction

Silicon vacancy centers (SiV centers) in diamonds have attracted attention for quantum information processing applications due to their high brightness, high photostability, and narrow zero-phonon line (ZPL) [1]. They exhibit a lifetime-limited linewidth [2] and indistinguishable photon emission [3]. In addition, they have all-optical accessible electronic spin [4, 5], which makes them promising candidates for quantum spin memory [6]. The electronic state of SiV centers exhibits high susceptibility to environmental strain, which leads to a longer spin coherence time [7, 8].

Nanodiamonds that contain single SiV centers are attractive in terms of coupling with various types of nanophotonics devices, such as photonic crystal cavities [9, 10], optical nanofibers [11–13], and nanofiber Bragg cavities [14–18], using bottom-up approaches. One method for the production of nanodiamonds that contain SiV centers is milling polycrystalline diamonds synthesized by chemical vapor deposition [19, 20]. Samples produced in this way exhibited narrow ZPL emission peaks (0.1 nm at 30 K) [19]. However, this method requires complex post-processing, such as acid treatment cleaning and centrifugation for size selection, after the milling process, such as bead-assisted sonic disintegration [19] and wet milling [20]. An alternative method to directly produce nanodiamonds with SiV centers is the synthesis of high-pressure high-temperature (HPHT) [21, 22].

Recently, another alternative method to efficiently create nanodiamonds containing SiV centers has been reported. In this method, SiV centers were formed by Si ion implantation into nanodiamonds followed by subsequent annealing in a vacuum at high temperature [23, 24]. SiV centers produced using this method have been reported to exhibit an emission linewidth as narrow as 6 nm at room temperature [23]. The formation of a single SiV center using this method has also been recently reported [24]. This method will make it possible to efficiently create SiV centers in small nanodiamonds, which is important for the low-loss coupling with nanophotonics devices. However, the optical properties of SiV centers in nanodiamonds created by this efficient method have not yet been reported at cryogenic temperatures. Investigating these properties is crucial for photonic quantum applications using a hybrid system between single SiV centers and nanophotonics devices.

In this work, we report a spectrometer-resolution-limited linewidth emission for a single SiV center produced by Si ion implantation of a commercial HPHT nanodiamond with an ion fluence of $5 \times 10^{11}\mathrm{ions cm}^{-2}$ and annealing at high temperature(up to 1100 °C) in a vacuum. Emission was observed from a single SiV center ($g^2(0) = 0.19$) with four distinct fine splittings of the ZPL at 4 K. The full width at half maximum (FWHM) of the ZPL reached the spectrometer resolution limit (0.09 nm) at an excitation power of 50 μW. To confirm that the emission comes from a single SiV center, we evaluated the temperature dependence and polarization dependence. As a result, the polarization dependence and temperature dependence of the emission peak are consistent with that of the emission coming from an SiV center under high strain. The results obtained in this work suggest that nanodiamonds containing single SiV centers formed using this method will be an important building block for the realization of quantum information applications.

2. Sample preparation

An HPHT nanodiamond suspension (Microdiamant, Pureon; MSY 0-0.1 (median size of 50 nm)) was purified by centrifugation (14 000 rpm for 30 min) to remove contaminants and small amounts of the suspension were spin-coated on silicon substrates. Si ions were then implanted into the nanodiamond samples with an acceleration energy and ion fluence of 30 keV and $5 \times 10^{11}\mathrm{ions\,cm}^{-2}$, respectively. The specific ion fluence was chosen based on the observation that emission from ensemble SiV centers was only observed at an ion fluence of $1 \times 10^{13}\mathrm{ions\,cm}^{-2}$ in our previous study [23].

After ion implantation, the samples were annealed in vacuum to form SiV centers in the nanodiamonds [23, 25]. The following annealing step was used: (1) 4 h at 400 °C under vacuum ($< 10^{-4}$ Pa); (2) 8 h at 800 °C under vacuum ($<10^{-4}$ Pa); (3) 1 h at 520 °C in air; (4) 4 h at 400 °C under vacuum ($< 10^{-4}$ Pa); (5) 2 h at 1100 °C under vacuum ($<10^{-4}$ Pa). Slow temperature ramping (>35 °C per hour) was used during steps (2) and (5). After annealing the sample, the samples were again heated at 520 °C for approximately 2 h in air to remove sp^2 carbon and surface contaminants.

After annealing, the nanodiamonds on the silicon substrate were dispersed in Milli-Q water by sonication. Small amounts of the suspension were drop-cast onto an Ir-coated substrate, upon which bright emission from SiV centers has been reported [26].

3. Experimental setup

An in-house-built cryogenic confocal microscope was used to measure the optical properties of SiV centers at cryogenic temperatures. Figure 1 shows the setup of the confocal microscope. The SiV centers were excited using a 685 nm continuous wave laser. The laser beam was filtered using a 685 nm bandpass filter and a 715 nm short-pass filter. It was focused on the sample in a liquid helium flow cryostat (Oxford) by an objective lens with numerical aperture (N.A.) of 0.7 (Olympus, LCPlanFL N, 50×). The sample was scanned by a galvano mirror and a 4f-lens system. The fluorescence from the sample was collected by the same objective lens and coupled to multimode fiber after being separated from the excitation laser by a dichroic mirror and a long-pass filter. After passing through an optical fiber, the fluorescence was measured by a single photon counting module (SPCM) and a spectrometer to acquire confocal images and emission spectra, respectively. To measure the second-order correlation function $g^2(\tau)$, the light path was able to be changed from the spectrometer to SPCM by the flip mirror. Regarding polarization dependence measurement, to change the polarization of the excitation laser, the half-wave plate was inserted in front of the dichroic mirror and to change the detection polarization, the polarizer was inserted in front of the fiber coupler. In the excitation power and polarization dependence measurement, photon counts were measured by one SPCM for about 5 s at 10 ms integration.

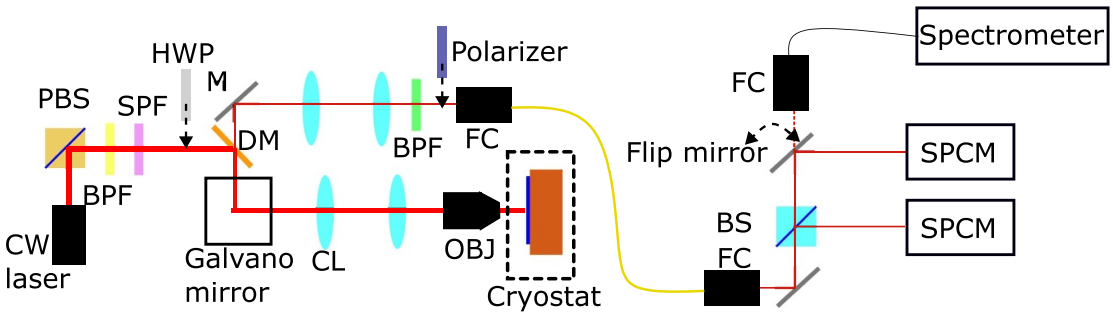

Figure 1. Schematic diagram of confocal microscope. PBS: polarized beam splitter. BPF: bandpass filter. HWP: half-wave plate. SPF: short-pass filter. DM: dichroic mirror. CL: concave lens. OBJ: objective lens. M: mirror. FC: fiber coupler. BS: beam splitter. SPCM: single photon counting module.

4. Experimental results

4.1. Emission spectrum from single SiV center in nanodiamond at 4 K

Figure 2(a) shows a confocal image of the sample at 4 K. There are several bright spots with various photon counts. From a second-order autocorrelation measurement, the brightest spot at the left bottom contained multiple emitters. We selected a relatively dim spot at the top right indicated by the blue circle.

Figure 2(b) shows a second-order autocorrelation function ($g^2(\tau)$) of the bright spot in the blue circle shown in figure 2(a). Slight bunching effect was observed in the data indicated by blue dots, which can be attributed to the shelving state [26]. Therefore, for analysis, we used a background-corrected three-level model of $g^2(\tau) = 1 + p_f^2(-(1+a)\exp(-\tau/\tau_1) + a\exp(-\tau/\tau_2))$ [27]. Here, p_f indicates the ratio of the photon counts from the SiV center to total counts, τ_1, τ_2 corresponds to the lifetime of the antibunching and bunching, and a describes the amplitude of the bunching. From the fitting, $g^2(0) = 0.19 < 0.5$ was acquired, which indicates that the emission is from a single SiV center. The non-zero $g^2(0)$ value was caused by background emission from the nanodiamond and the timing jitter of the measurement equipment. The fitting with the parameters p_f, τ_1, τ_2, and a of 0.90, 1.3 ns, 9.8 ns, and 0.10, respectively, is in good agreement with the data as shown in figure 2(b). From the fitting parameters, the lifetime of the excited state is estimated to be 1.3 ns, which is consistent with the lifetime of the excited state of single SiV centers in nanodiamonds produced by HPHT synthesis at cryogenic temperature [21]. Please note that this value includes the effect of jitter, therefore the actual lifetime can be smaller than this value.

Figure 2(c) shows the emission spectrum with the excitation power of 10 mW from the bright spot in the blue circle shown in figure 2(a). A sharp peak is observed at around 736.7 nm, and 2nd peak is observed at around 735.8 nm. In addition, the peaks with small intensity are observed at around 738.7 nm and 733.8 nm, which are shown in figure 2(c) at 50× (red line) and 100× (purple line) magnification, respectively, for ease of viewing.

To show that the spectral splitting is consistent with the electronic structure shown in figure 2(d), we calculated the splitting of the ground state and excitation state from the peak positions. The peak positions were deduced to be 733.79 ± 0.01 nm (A), 735.78 ± 0.01 nm (B), 736.65 ± 0.01 nm (C), and 738.68 ± 0.01 nm (D) by Gaussian fitting. The ZPL position, which is defined as the average of the four peak wavelengths was calculated to be 736.22 nm. The peaks A to D correspond to the transitions A to D, which are attributed to splitting in the excited state and the ground state by spin-orbit interaction, as shown in figure 2(d). The splittings of the ground (Δ_{GS}) and excited states (Δ_{ES}) calculated from the emission spectrum were ∼1.12 THz ($\omega_A - \omega_B = 1.12 \pm 0.02$ THz, $\omega_C - \omega_D = 1.11 \pm 0.02$ THz) and ∼1.59 THz ($\omega_A - \omega_C = 1.59 \pm 0.02$ THz, $\omega_B - \omega_D = 1.58 \pm 0.02$ THz), respectively. These splittings are almost similar to those for SiV centers formed by Si ion implantation in a diamond-cavity with $\Delta_{GS} > 1$ THz [8]. The splittings of the ground and excited state are highly susceptible to local strain (∼1 PHz/strain) [7, 28]. The origin of this high strain could be damage due to ion implantation or the stress caused by crushing. Therefore, it can be concluded that these 4 peaks in figure 2(c) can be explained by the electronic structure shown in figure 2(d), which is consistent with the emission from SiV center under high strain.

4.2. Excitation power dependence of SiV center emission at 4 K

In order to investigate the intrinsic linewidth of peak C, we measured the spectra with changing the excitation laser power.

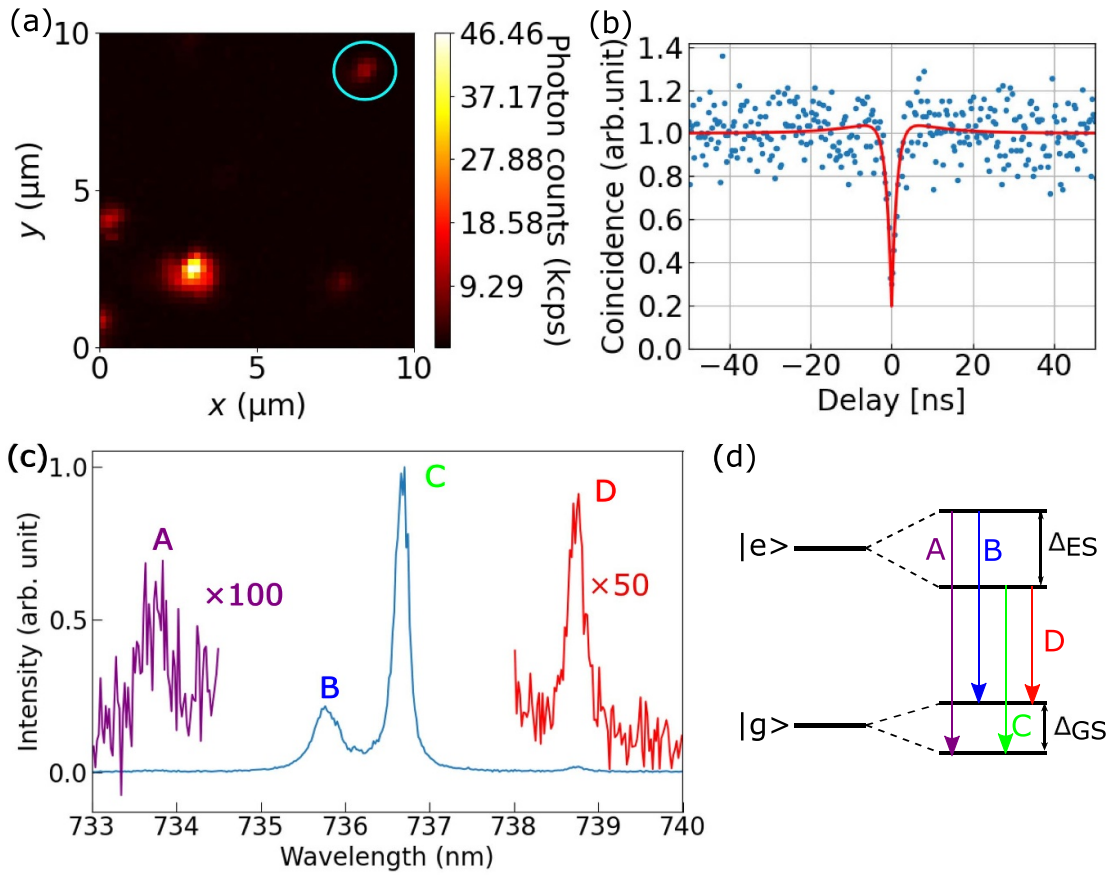

Figure 2. (a) Confocal image of sample at 4 K. (b) Second-order autocorrelation function $g^2(\tau)$. $g^2(0) = 0.19$ indicates that the bright spots contain a single SiV center. (c) Emission spectrum from bright spot in blue circle shown in (a). For clarity, the purple and red lines show the intensities around peaks A and D multiplied by a factor of 100 and 50, respectively. (d) Schematic image of electronic structure of SiV center. The splitting was caused by spin-orbit interaction. The transitions A to D correspond to the peaks A to D shown in (c).

Figure 3(a) shows the emission spectrum in the wavelength range between 735 nm and 738 nm, which includes peaks B and C, when the excitation power is 10 mW (blue), 1 mW (orange), and 50 μW (green). For clarity, the emission spectra measured with excitation powers of 1 mW and 50 μW are multiplied by 4 and 80, respectively. The excitation power was measured in front of the objective lens. When the excitation power decreased, the linewidth of the peaks became narrower. The FWHMs of peak C were 0.27 nm, 0.14 nm, and 0.09 nm when the excitation power was 10 mW, 1 mW, and 50 μW, respectively. The FWHM of 0.09 nm is the resolution limit of the spectrometer determined by measurement of the emission spectrum of an argon lamp. Therefore, we believe the actual linewidth at an excitation power of 50 μW is much smaller than 0.09 nm. Also, as the excitation power decreased, the peak position blue-shifted. The decrease in linewidth and blue-shift of the peak with decreasing excitation power are considered to be due to the decrease in local heating by the excitation laser [29], which is also consistent with the temperature dependence in section 4.4.

Figure 3(b) shows the photon counts as a function of excitation power. As the excitation power increased, the photon counts increased, however, the photon count rate approached saturation at around an excitation power of 15 mW. We fitted an equation given by $I = I_\infty \times P/(P + P_{\mathrm{sat}})$ to the data, as shown in the red line of figure 3(b), where I is the photon count, P is the excitation power in front of the objective lens, and I_∞ (maximum count) and P_{sat} (saturation power) are fitting parameters [30]. The data are in good agreement in the fitting. The I_∞ and P_{sat} obtained from the fitting were 85 kcps and 29 mW, respectively.

4.3. Polarization dependence of SiV center emission at 4 K

The polarization dependence of SiV center emission at 4 K was measured to confirm that the emission shown in figures 2 and 3 was from a single SiV center.

Orange dots in figure 4(a) show the photon counts for the SiV center shown in figure 2 as a function of the excitation polarization. The 0° is the polarization angle at which the data in figures 2 and 3 were measured. We fitted the equation $a\cos^2(b\theta + c) + d$ to the data as indicated by the black line in figure 4(a), where θ is the polarization angle of the excitation laser, and a, b, c, and d are fitting parameters. From the

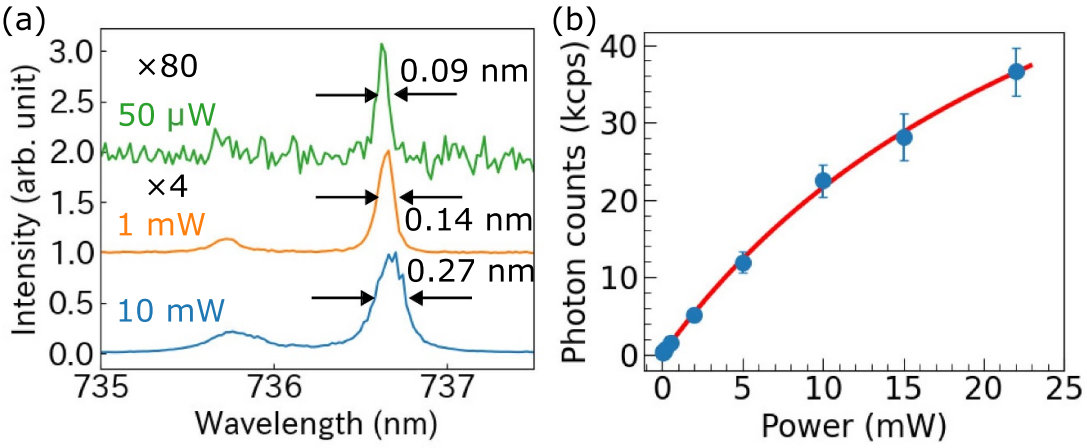

Figure 3. (a) Excitation power dependence of emission spectra in range of 735 nm to 738 nm. The excitation power is 50 μW(green), 1 mW (orange), and 10 mW (blue) in front of the objective lens. (b) Photon count for bright spot in blue circle shown in figure 2(a) as function of excitation power. Error bars indicate the standard deviation. The red line shows the fitting.

fitting, the angle at which the photon counts are maximized is 22° and visibility is 37%. This low visibility might be due to the dipole orientation and non-resonant excitation.

Blue dots in figure 4(a) show the photon counts from the bright spot in the blue circle in figure 2(a) as a function of the detection polarization. Please note that the excitation polarization was set to 22°. We fitted the same function mentioned in the previous paragraph to the data as indicated by the red line in figure 4(a). From the fitting, the angle at which the photon counts are maximal is 22° and visibility is 83%. The excitation polarization angle at which the photon counts are maximized is the same as the detection polarization angle, which is consistent with the previous study [31].

The upper panel and lower panel in figure 4(b) show emission spectra of the SiV center shown in figure 2 when the detection polarization was set to 22° and 112° at which the photon counts are maximized and minimized, respectively. For clarity, the spectra are shown with the intensity offset of 0.2 and multiplied by 50 in the 733 nm to 734.5 nm range and by 100 in the 738 nm to 740 nm range. In the upper panel of figure 4(b), peaks B and C are clearly observed and in the lower panel, the intensity of the peaks is greatly decreased. On the other hand, the intensity of the peaks A and D remained almost unchanged. The dipoles of transitions A and D have been reported to be perpendicular to B and C [22, 32, 33] and the polarization contrast for each peak is reported to be highly dependent on the orientation of the nanodiamonds [21]. These results suggest that the dipoles of transitions B and C are in a plane perpendicular to the excitation laser beam, whereas the dipoles of transitions A and D are almost parallel to the beam. This assumption is consistent with the intensities of peaks A and D being one to two orders of magnitude smaller than those of peaks B and C, as shown in figure 2(c).

Therefore, it can be concluded that the direction of the excitation polarization coincides with the excitation polarization that maximizes the emission intensity and transitions A and D possess a different orientation dipole to transitions B and C, which is consistent with the polarization dependence of the emission from a single SiV center.

4.4. Temperature dependence of SiV center emission

The temperature dependence of the SiV center emission was measured to confirm that the 4 peaks in figure 2(c) come from a single SiV center. In this measurement, the excitation laser power was set to 5 mW to suppress the broadening of the FWHM by the high excitation laser power and to acquire a sufficient photon count to measure the emission spectra.

Figure 5(a) shows emission spectra for the SiV center shown in figure 2(c) at 4, 40, 100, and 250 K. For ease of viewing, the 100 K and 250 K spectra are multiplied by factors of 5 and 20, respectively. The ZPL position showed a red-shift and the linewidth increased with increasing temperature.

Figure 5(b) shows the temperature dependence of the FWHM of peak C in the spectrum shown in figure 2(c) from 4 K to 270 K. Below 100 K, the FWHM was calculated using two Gaussians to distinguish between peaks B and C. On the other hand, above 150 K, they merged into one, therefore a single Gaussian was used to calculate the FWHM. The range of change in the FWHM is from $\sim$ 100 GHz to $\sim$ 3.0 THz. The data below 80 K were fitted using $\alpha_1 \exp(-h\Delta_{ES}/k_B T)$ (red line) and the data above 100 K were fitted using $\alpha_1 \exp(-h\Delta_{ES}/k_B T) + \alpha_2 T^3$ (green line), where h is the Planck constant, k_B is the Boltzmann constant, T is

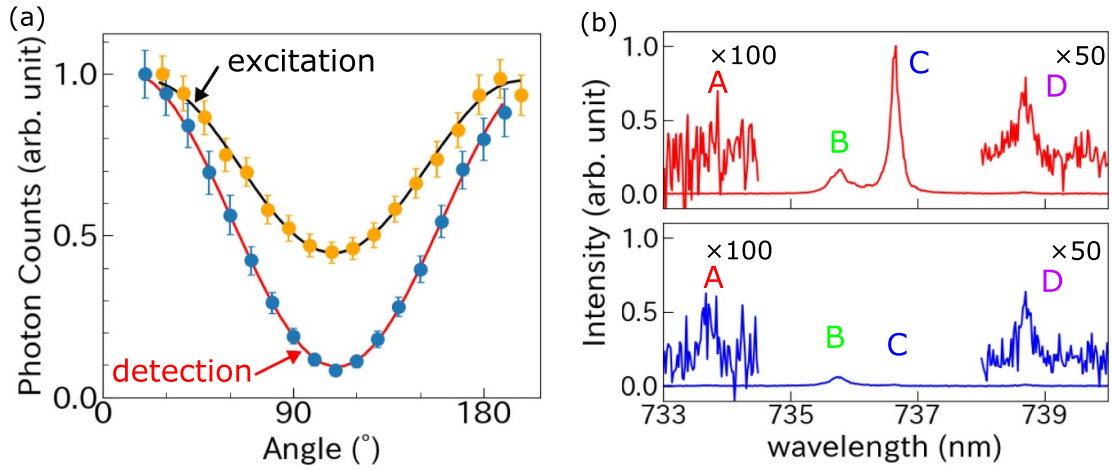

Figure 4. (a) Photon count rate as a function of excitation polarization (orange dots and black line) and detection-polarization (blue dots and red line). The error bars indicate the standard deviation. (b) Emission spectra when detection polarization is set to 22° (Upper panel) and 112° (Lower panel), which correspond to the angle at the maximum and minimum intensity in (a), respectively. Note that intensity of upper panel and lower panel is normalized by the same value.

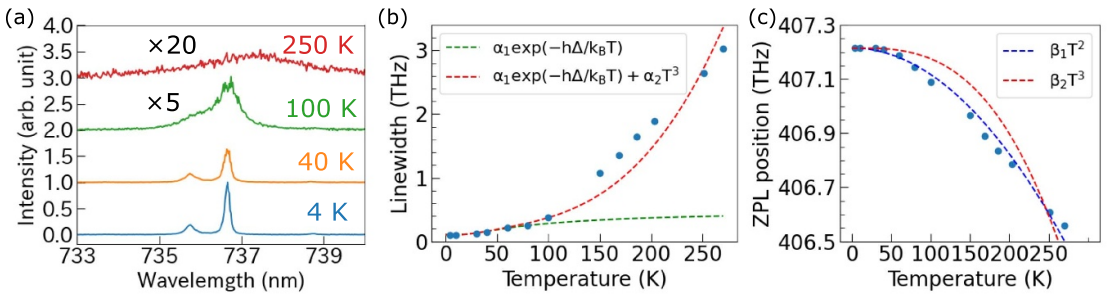

Figure 5. (a) Emission spectra at 4 K (blue), 40 K (yellow), 100 K (green), and 250 K (red) with an excitation power of 5 mW. (b) Temperature dependence of FWHM of peak C. The green and red lines are the fits using $\alpha_1 \exp(-h\Delta_{ES}/k_B T)$ and $\alpha_1 \exp(-h\Delta_{ES}/k_B T) + \alpha_2 T^3$, respectively. (c) Temperature dependence of ZPL position (center of peaks A to D). The blue and red lines are fits using $\beta_1 T^2$ and $\beta_2 T^3$, respectively.

the temperature, and α_1 and α_2 are fitting parameters. The temperature variation of the linewidth is considered to result from electron-phonon coupling [34, 35]. For a SiV center, when the thermal energy is almost the same as the excited state splitting ($h\Delta_{ES} \sim k_B T$), the first-order electron-phonon process ($\alpha_1 \exp(-h\Delta_{ES}/k_B T)$ dependence) is dominant, and when the thermal energy is greater than the excited state splitting ($k_B T \gg h\Delta_{ES}$), the second-order electron-phonon process (T^3 dependence) is dominant [7, 35]. In this sample, Δ_{ES} is $\sim$ 1.59 THz, which corresponds to $\sim$ 76 K. Therefore, the first-order electron-phonon coupling model ($\alpha_1 \exp(-h\Delta_{ES}/k_B T)$) was used to the data below 80 K and a linear combination of first-order and second-order electron-phonon coupling models ($\alpha_1 \exp(-h\Delta_{ES}/k_B T) + \alpha_2 T^3$) was used to the data above 100 K, where α_1 and α_2 are fitting parameters. Above 100 K, the data deviate from the $\alpha_1 \exp(-h\Delta_{ES}/k_B T) + \alpha_2 T^3$ fit; this trend has also been observed in previous studies [34, 35]. This is thought to be because above 150 K the FWHM is calculated by combining four peaks. On the other hand, below 80 K the $\alpha_1 \exp(-h\Delta_{ES}/k_B T)$ with the Δ_{ES} calculated from the spectrum shown in figure 2(c) is in good agreement with the data, which is strong evidence that the 4 peaks in figure 2(c) come from single SiV center.

Figure 5(c) shows the temperature dependence of the ZPL position (the center of 4 peaks). To calculate the ZPL position, the emission spectra were fitted with four Gaussian functions below 60 K, two Gaussian functions at 80 K and 100 K, and a single Gaussian function above 120 K. This is because the A and D peaks are too weak above 80 K, and the four peaks merged into one peak above 120 K. The ZPL position changed from 407.2 THz (4 K) to 406.6 THz (270 K). The ZPL shift in figure 5(c) was fitted by equations $\beta_1 T^2$ and $\beta_2 T^3$, where β_1 and β_2 are fitting parameters. The shift of the ZPL position is considered to result from thermal expansion of the diamond lattice (T^2 dependence) and an electron-phonon coupling process (T^3 dependence) [35]. A comparison of the T^2 and T^3 fits revealed that the T^2 fit is in better agreement with the data. The ZPL position in the present sample is considered to be mainly determined by thermal expansion, which is consistent with the temperature dependence of the ZPL shift for a SiV center [34].

Therefore, it can be concluded that the four peaks come from a single SiV center by analyzing the temperature dependence of the line width using the electron-phonon coupling model. Furthermore, it can be concluded that the temperature variation of the ZPL position originates from expansion of the diamond lattice, which is consistent with the temperature dependence of the emission from a SiV center.

5. Discussion

According to the analysis in sections 4.2–4.4, we confirm that the narrow emission peak in the spectrum shown in figure 2(c) comes from a single SiV center. In this study, we investigated the optical properties of small nanodiamonds (approximately 50 nm) at cryogenic temperatures from the perspective of efficient coupling to nanophotonic devices. A relevant study has reported on the optical properties of single SiV centers in nanodiamonds of similar size, which produced HPHT treatment with Si-doping components [21]. This study measured a narrow emission linewidth of 142 MHz using photoluminescence excitation (PLE). Compared to this method, our approach using ion implantation into preselected nanodiamonds offers the advantage of efficient creation of SiV center in nanodiamonds with uniform size due to its controllability of the ion implantation process.

In this study, we observed that the emission from the SiV center showed a spectrometer resolution limit linewidth of 0.09 nm, which indicates the intrinsic linewidth of the emission should be much smaller than 0.09 nm. Therefore, to measure the intrinsic linewidth with higher precision, PLE measurements are important for future works.

6. Conclusion

Single SiV centers were formed in nanodiamonds by Si ion implantation and exhibited an emission linewidth that was limited by the spectrometer resolution. The nanodiamonds were evaluated at cryogenic temperatures and the emission observed from a single SiV center had four distinct fine structure peaks. The emission line FWHM was at the spectrometer resolution limit (0.09 nm) when the excitation power was 50 μW. In the polarization dependence measurement, the detection polarization angle of maximum intensity was verified to coincide with the excitation polarization angle. Emission spectra were measured with two orthogonal polarizations, which indicated that the orientations of the emission diploes of peaks A and D are different from those of peaks B and C. Emission spectra were measured from 4 K to 270 K and the temperature dependence of the linewidth and the ZPL position was evaluated. The temperature dependence of the linewidth could be described by a first-order electron-phonon coupling model ($\alpha_1 \exp(-h\Delta_{ES}/k_B T)$ dependence) below 100 K and a linear combination of first-order and second-order electron-phonon coupling models (T^3 and $\alpha_1 \exp(-h\Delta_{ES}/k_B T)$ dependence) above 150 K. These results are consistent with the emission properties of SiV centers. The narrow emission peaks observed suggest that nanodiamonds containing single SiV centers produced using this method could be important building blocks for quantum information technology. Towards the realization of high-efficiency single photon sources, the coupling of nanodiamonds containing single SiV centers to nanophotonics devices at cryogenic temperatures will be the subject of our future work.

Data availability statement

The data cannot be made publicly available upon publication because no suitable repository exists for hosting data in this field of study. The data that support the findings of this study are available upon reasonable request from the authors.

Acknowledgments

The authors gratefully acknowledge financial support in the form of Kakenhi Grants-in-Aid (Nos. 24H00195, 21H04444, 26220712, 23K22426, and 19K03686) from the Japan Society for the Promotion of Science (JSPS), the CREST program of the Japan Science and Technology Agency (JST) (JPMJCR1674), the Ministry of Education, Culture, Sports, Science and Technology (MEXT) Quantum Leap Flagship Program (MEXT Q-LEAP) (JPMXS0118067634), and the support of the Matsuo Foundation and the JST PRESTO program (Grant Number JPMJPR2257).

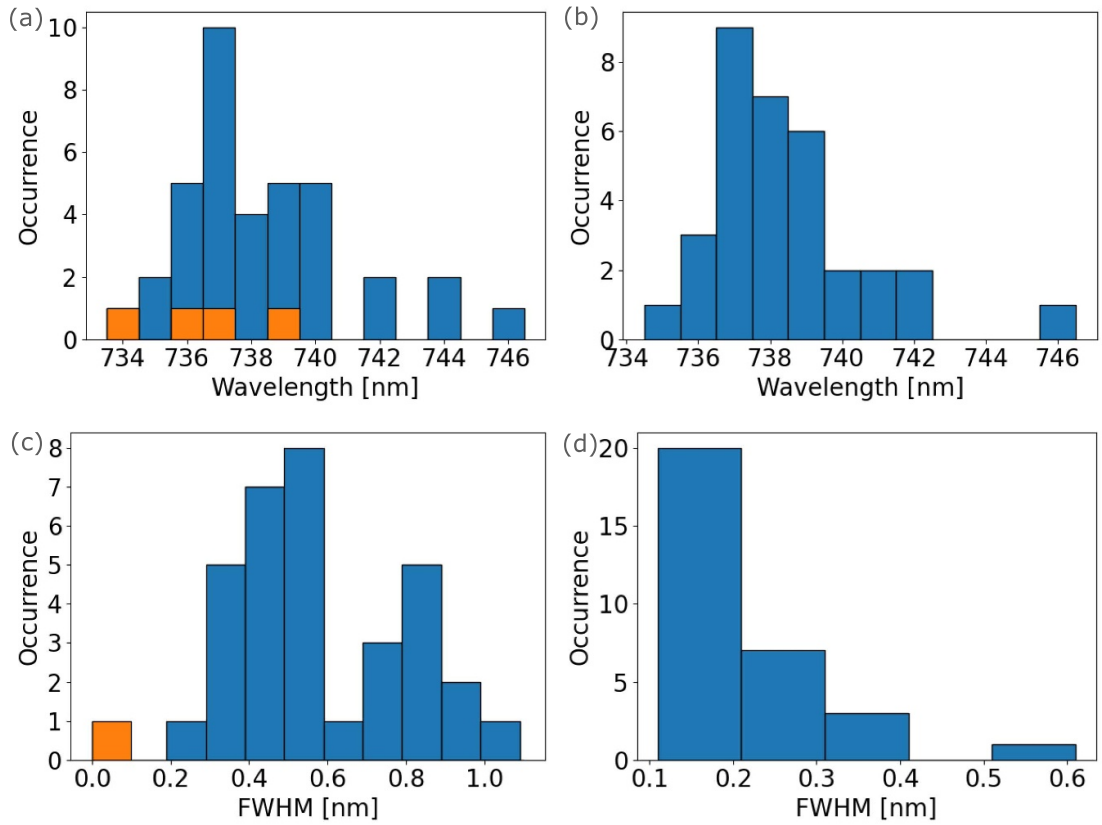

Figure A1. Size-dependence of the peak wavelength and FWHM at 4 K (a) and (b) shows the histogram of the distribution of the ZPL peak position for MSY 0.1 (median size is 50 nm) with ion fluence of 5×10^{11}ionscm^{-2} and MSY 0.5 (median size is 210 nm) with ion fluence of 5×10^{12}ionscm^{-2}, respectively. The orange lines indicate the data shown in figure 2(c). (c) and (d) shows the histogram of the distribution of FWHM of the ZPL peaks for MSY 0.1 and MSY 0.5, respectively. The orange line shows FWHM shown in figure 3(a). Note that FWHM values shown by blue lines can be broadened due to the high excitation laser power and including ensemble emission.

Appendix

In this appendix, we show the size-dependent spectral properties. Figure A1 shows the histogram of the distribution of ZPL peak wavelength and the FWHM for MSY 0.1 (median size is 50 nm) with ion fluence of 5×10^{11} and MSY 0.5 (median size is 210 nm) with ion fluence of 5×10^{12}. In both of the samples, the ZPL peak position ranges from 734 nm to 746 nm, which suggests that the internal strain does not depend on nanodiamond size. On the other hand, as expected, the FWHM of the peaks tends to be smaller in the larger nanodiamonds. Please note that the FWHM data shown in figure A1 can be broadened by the high excitation laser power of 23 mW and broadening by ensemble emission.

ORCID iDs

Konosuke Shimazaki https://orcid.org/0009-0002-7632-3175
Kazuki Suzuki https://orcid.org/0009-0008-4756-6200
Kengo Sakamoto https://orcid.org/0009-0009-9580-9139
Yudai Okashiro https://orcid.org/0009-0005-3372-5192
Hiroshi Abe https://orcid.org/0000-0001-9659-8382
Takeshi Ohshima https://orcid.org/0000-0002-7850-3164
Hideaki Takashima https://orcid.org/0000-0002-2398-815X
Shigeki Takeuchi https://orcid.org/0000-0001-7731-003X

References

[1] Bradac C, Gao W, Forneris J, Trusheim M E and Aharonovich I 2019 *Nat. Commun.* **10** 1–13
[2] Li K, Zhou Y, Rasmita A, Aharonovich I and Gao W B 2016 *Phys. Rev. Appl.* **6** 024010
[3] Sipahigil A, Jahnke K D, Rogers L J, Teraji T, Isoya J, Zibrov A S, Jelezko F and Lukin M D 2014 *Phys. Rev. Lett.* **113** 113602

[4] Rogers L J et al 2014 Phys. Rev. Lett. 113 263602
[5] Sukachev D D, Sipahigil A, Nguyen C T, Bhaskar M K, Evans R E, Jelezko F and Lukin M D 2017 Phys. Rev. Lett. 119 223602
[6] Bhaskar M K et al 2020 Nature 580 60–64
[7] Meesala S et al 2018 Phys. Rev. B 97 205444
[8] Stas P J et al 2022 Science 378 557–60
[9] Fehler K G, Ovvyan A P, Antoniuk L, Lettner N, Gruhler N, Davydov V A, Agafonov V N, Pernice W H P and Kubanek A 2020 Nanophotonics 9 3655–62
[10] Wolters J, Schell A W, Kewes G, Nüsse N, Schoengen M, Döscher H, Hannappel T, Löchel B, Barth M and Benson O 2010 Appl. Phys. Lett. 97 141108
[11] Fujiwara M, Toubaru K, Noda T, Zhao H Q and Takeuchi S 2011 Nano Lett. 11 4362–5
[12] Schell A W, Takashima H, Tran T T, Aharonovich I and Takeuchi S 2017 ACS Photonics 4 761–7
[13] Yalla R, Kojima Y, Fukumoto Y, Suzuki H, Ariyada O, Shafi K M, Nayak K P and Hakuta K 2022 Appl. Phys. Lett. 120 241102
[14] Schell A W, Takashima H, Kamioka S, Oe Y, Fujiwara M, Benson O and Takeuchi S 2015 Sci. Rep. 5 1–5
[15] Tashima T, Takashima H, Schell A W, Tran T T, Aharonovich I and Takeuchi S 2022 Sci. Rep. 12 1–7
[16] Li W, Du J and Chormaic S N 2018 Opt. Lett. 43 1674–7
[17] Takashima H, Fukuda A, Maruya H, Tashima T, Schell A W and Takeuchi S 2019 Opt. Express 27 6792–800
[18] Romagnoli P, Maeda M, Ward J M, Truong V G and Chormaic S N 2020 Appl. Phys. B 126 1–16
[19] Neu E et al 2011 Appl. Phys. Lett. 98 243107
[20] Lindner S, Bommer A, Muzha A, Krueger A, Gines L, Mandal S, Williams O, Londero E, Gali A and Becher C 2018 New J. Phys. 20 115002
[21] Haußler S, Hartung L, Fehler K G, Antoniuk L, Kulikova L F, Davydov V A, Agafonov V N, Jelezko F and Kubanek A 2019 New J. Phys. 21 103047
[22] Rogers L J, Wang O, Liu Y, Antoniuk L, Osterkamp C, Davydov V A, Agafonov V N, Filipovski A B, Jelezko F and Kubanek A 2019 Phys. Rev. Appl. 11 024073
[23] Takashima H et al 2021 Opt. Mater. Express 11 1978–88
[24] Xu X et al 2023 Nanophotonics 12 485–94
[25] Shimazaki K, Kawaguchi H, Takashima H, Segawa T F, So F T-K, Terada D, Onoda S, Ohshima T, Shirakawa M and Takeuchi S 2021 Phys. Status Solidi a 218 2100144
[26] Neu E, Agio M and Becher C 2012 Opt. Express 20 19956–71
[27] Kurtsiefer C, Mayer S, Zarda P and Weinfurter H 2000 Phys. Rev. Lett. 85 290
[28] Sternschulte H, Thonke K, Sauer R, Münzinger P C and Michler P 1994 Phys. Rev. B 50 14554
[29] Gao Y, Lai J M, Li Z Y, Tan P H, Shan C X and Zhang J 2024 Appl. Phys. Lett. 124 91101
[30] Neu E, Steinmetz D, Riedrich-Möller J, Gsell S, Fischer M, Schreck M and Becher C 2011 New J. Phys. 13 025012
[31] Neu E, Fischer M, Gsell S, Schreck M and Becher C 2011 Phys. Rev. B 84 205211
[32] Hepp C et al 2014 Phys. Rev. Lett. 112 036405
[33] Rogers L J et al 2014 Phys. Rev. B 89 235101
[34] Neu E, Hepp C, Hauschild M, Gsell S, Fischer M, Sternschulte H, Steinmüller-Nethl D, Schreck M and Becher C 2013 New J. Phys. 15 043005
[35] Jahnke K D, Sipahigil A, Binder J M, Doherty M W, Metsch M, Rogers L J, Manson N B, Lukin M D and Jelezko F 2015 New J. Phys. 17 043011